Spatiotemporal filamentary patterns in a dc-driven planar gas discharge system

C. Strümpel and H.-G. Purwins
Institute of Applied Physics, Münster University, Corrensstrasse 2/4, D-48149 Münster, Germany

Yu. A. Astrov
A. F. Ioffe Physico-Technical Institute, Russian Academy of Sciences, St. Petersburg 194021, Russia

(Received 23 August 2000; published 24 January 2001)

In a dc-driven planar gas discharge system with a semiconductor electrode, the homogeneous stationary discharge state can be destabilized in favor of current filaments. A filament consists of a succession of spatially confined breakthroughs of the gas layer that repeatedly take place at approximately the same position. A pulsating filament is thus slowly moving over the active area of the system. At fixed parameters, processes of creation and quenching of filaments are observed, while their average spatial density depends on control parameters. Depending on the density, filaments arrange in different configurations. At an intermediate value of filament density, a pattern on a two-dimensional domain is found: it is a spatially anisotropic chain pattern that is specified by two characteristic spatial scales. It is suggested that the observed phenomena are due to a Hopf-Turing instability arising in the system.

DOI: 10.1103/PhysRevE.63.026409 PACS number(s): 52.80.−s, 05.65.+b, 45.70.Qj

I. INTRODUCTION

Spatiotemporal self-organization of nonlinear dissipative systems is a well-known phenomenon [1–3]. It has been investigated in systems of different origins, such as chemical [4–6], biological [7,8], and physical systems [9,10]. Among the emerging patterns, one can distinguish between periodic patterns like Turing stripe patterns and solitary objects, also known as quasiparticles [11,12]. In cryogenic planar gas-discharge systems with semiconductor electrode, both kinds of patterns have been shown to exist [13–20]. The solitary structures in the gas discharge are filaments of electric current. In some aspects, they behave like quasiparticles. They can interact with each other and form ''molecules'' or larger clusters [18]. While the filaments are able to move across the gas discharge area, they carry a time-independent current.

A qualitative description of pattern-forming processes can be given in many cases by reaction-diffusion equations. The solutions of such equations include Turing and Hopf patterns and their mixed modes as well as solitary objects. This approach can also be applied to planar gas-discharge systems with a semiconductor electrode [13,21]. The behavior of current filaments in cryogenic gas-discharge systems agrees in a qualitative manner with the properties of quasiparticles that are found in coupled reaction-diffusion systems.

In the present experimental work, a planar semiconductor dc-driven gas-discharge system at room temperature has been used. In contrast to the cryogenic systems, the leading destabilization of the stationary homogeneous low current-density (reference) state has been found to be the instability that gives rise to a spatial homogeneous oscillation [22]. This oscillatory state can be destabilized through the appearance of a small number of oscillating current filaments, which then coexist with their oscillating background. The discussion of such phenomena shall be given in a detailed manner in another paper. On the other hand, for the case of low conductivity of the semiconductor electrode (typically three times smaller than for the oscillatory case), a direct transition from the reference state to complicated spatiotemporal patterns is observed, without the intermediate state of homogeneous oscillation. Spatial patterns that are stationary in time have not been found in the parameter range considered in this work. In this contribution, emerging spatiotemporal filaments and their creation and disappearance processes are investigated. Depending on the average number—which can be influenced by the control parameters of the system—the filaments arrange in different spatial constellations. An investigation on a shorter time scale (of the order of μs) reveals the underlying temporal characteristics of filament patterns. Independent of the actual pattern that they form, the filaments consist each of a series of short and spatially confined breakthroughs. Due to the fact that the position of breakthroughs just moves slowly, the filaments become visible on a large time scale of the order of 1 s.

II. EXPERIMENTAL SETUP AND RESULTS

The experiments discussed in this work are carried out on a planar gas-discharge system with an active area of a maximum diameter of $D=30$ mm (cf. Fig. 1). One of the electrodes is fabricated from semi-insulating gallium arsenide with a thickness of $a_{\mathrm{GaAs}}=1.5$ mm. The other electrode is a metallic transparent indium tin oxide (ITO) layer that covers a glass plate. The discharge gap has a width of $d=0.5$ mm and is filled with nitrogen. The pressure p lies in the range between 40 and 60 hPa. The outer side of the semiconductor electrode is covered by a thin gold contact, which is approximately 40 nm thick. By applying a high voltage U_0 between the gold contact and the ITO layer, a discharge is ignited in the gap. The global discharge current I is measured through the voltage drop at a small serial resistor $R_I=100\,\Omega$. The voltage drop at this resistor (of the order of 100 mV) is negligible with respect to the supply voltage. The transparent ITO electrode allows a visual observation of the discharge

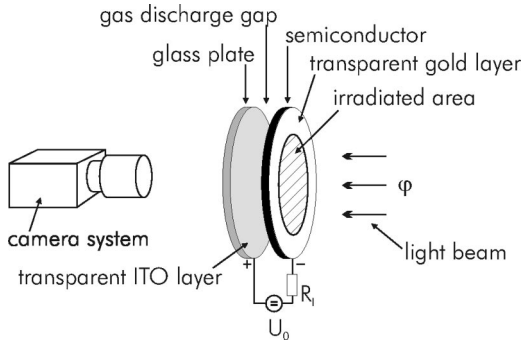

FIG. 1. Sketch of the experimental setup. The maximum diameter of the discharge area is 30 mm, the width of the gap is $d=0.5$ mm, and the thickness of the semiconductor electrode is $a_{\mathrm{GaAs}}=1.5$ mm. The gap is filled with nitrogen at a typical pressure p in the range of 40–60 hPa. The semiconductor electrode is irradiated by light with radiation flux density φ.

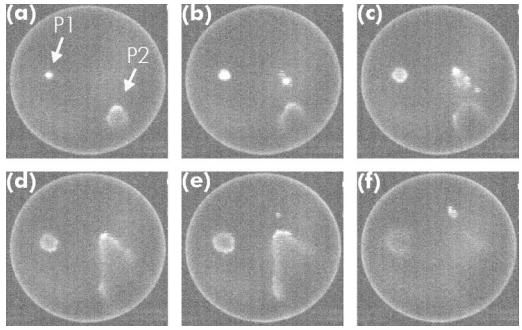

FIG. 2. A sequence of subsequent snapshots of the discharge glow in the state of moving wavelike structures taken with a frame repetition rate of $f_{rep}=25$ Hz. The exposure time of each snapshot is $t_{exp}=40$ ms. The experimental parameters are $U_0=655$ V, $\varphi=0.035$ [$\sigma_{\mathrm{GaAs}}=0.54\times10^{-7}$ $(\Omega\ \mathrm{cm})^{-1}$], and $p=60$ hPa.

glow. The pictures of the discharge are recorded with either a conventional charge coupled device camera or a gated light-intensified camera, which allows short exposure time. Due to the internal photoeffect, the specific conductivity of the gallium arsenide electrode can be manipulated by irradiation with light. This is possible because the gold contact on the outer surface of the electrode is transparent with respect to visible light, its transmission coefficient being about 10%. When the light is absorbed by the material of the semiconductor electrode, electrons from the valence band are excited into the conduction band. Hence, the specific conductivity is raised. The conductivity varies almost linearly with the intensity of the incoming light, which is used to irradiate the semiconductor. In the following we will present data that depend on the normalized radiation flux in the visible φ. When the gallium arsenide is not irradiated ($\varphi=0$), its specific conductivity is of the order of 3×10^{-8} $(\Omega\ \mathrm{cm})^{-1}$ [23]. For the maximum irradiation used in the present experiments ($\varphi=1$), a conductivity of 2.5×10^{-7} $(\Omega\ \mathrm{cm})^{-1}$ has been reached. When some parts of the semiconductor are irradiated and some are not, qualitatively different states of the discharge can be realized, e.g., nonirradiated areas being in a low-current state accompanied by low emission of light from the discharge gap. The homogeneously excited domains (called active areas) may be prepared in different spatial configurations by applying appropriate masks. Besides φ, the feeding voltage U_0 can be changed easily in the experiments. Therefore, these two quantities are used as the main control parameters. Other parameters like gas pressure p and discharge gap thickness d remain fixed or are changed discontinuously in a narrow range.

A typical development of the discharge can be observed in the device by varying the control parameters in the range of $U_0=400-1200$ V and $\varphi=0.03-0.12$. The corresponding specific conductivity of the semiconductor electrode then is in the range of $\sigma_{\mathrm{GaAs}}=(0.50-1.18)\times10^{-7}$ $(\Omega\ \mathrm{cm})^{-1}$. Under these conditions, a spatial homogeneous stationary discharge is ignited in the gas gap of the device at $U_0\approx400$ V. This state of low current discharge corresponds to the so-called Townsend discharge [24]. Raising the voltage in this mode leads to a linearly growing current, indicating the Ohmic behavior of the semiconductor electrode. The voltage at the gas gap is constant and independent of the discharge current in the Townsend mode. This discharge mode can be destabilized by a further increase in current that can be done by increasing either the feeding voltage or the irradiation of the semiconductor electrode. The resulting patterns in the current density that become visible in the distribution of the discharge glow are nonhomogeneous and nonstationary [25]. The nonstationarity is both spatial and temporal in nature. While the spatial aspects are considered in the following paragraphs, the discussion of the temporal aspects is given further below.

Just beyond the destabilization, a state organizes that is illustrated by the example given in Fig. 2. To demonstrate the dynamical properties of this state, a sequence of subsequent pictures (taken at a repetition rate $f_{rep}=25$ Hz with an exposure time $t_{exp}=40$ ms) is shown. At the point marked by $P1$ in Fig. 2(a), a filament has appeared. In the course of time [Figs. 2(b)–2(e)] it fades out, thereby retaining its circular symmetry. In Fig. 2(f), it is merely visible and a time step later it has vanished completely (not shown here). The situation at the point marked with $P2$ in Fig. 2(a) is somehow different. There, a solitary structure that has appeared, is almost a semicircular stripe. In the course of time, this stripe gets combined with other stripes resulting from the fading out of other filaments appearing in Figs. 2(b) and 2(c). This can be seen in Fig. 2(d). The resulting longer stripe also vanishes in Fig. 2(f). The speed of propagation of the described stripes is of the order of 10 mm/s.

Increasing the voltage far beyond $U_0=400$ V leads to a spatial stabilization of the originally fading-out filaments and the patterns that are observed in the gas-discharge area at higher voltages are composed of filaments that are spatially stable in the sense that they keep their shape in the course of time. The current density distribution corresponding to this situation is depicted in Figs. 3(a)–3(i). The corresponding time average of the discharge current in dependence of the supply voltage U_0 can be seen in Fig. 3(j). The discharge current grows due to the increase in the number of filaments. In Fig. 3(a) there is only a small number of filaments in the gas-discharge area. In this stage of the process, the filaments

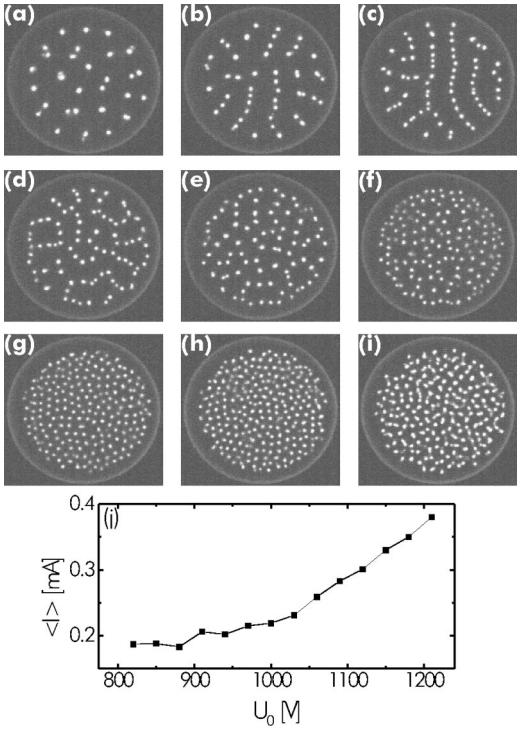

FIG. 3. Current density distribution in the gas discharge, the images are taken with $t_{exp}=40$ ms and the parameters $\varphi=0.05$ $[\sigma_{\mathrm{GaAs}}=0.65\times10^{-7}\ (\Omega\ \mathrm{cm})^{-1}]$, $D=25$ mm, and $p=42$ hPa. The respective feeding voltages U_0 are (a) 820 V, (b) 850 V, (c) 880 V, (d) 910 V, (e) 940 V, (f) 1000 V, (g) 1060 V, (h) 1120 V, and (i) 1210 V. In (j) the time average of the global discharge current is plotted as a function of the supply voltage U_0.

are moving in a random manner on the active area; the average velocity of this movement is of the order of 3 mm/s. Because of the relatively low velocity the filaments seem to be fixed in snapshots obtained with 40-ms exposure time. When U_0 increases, the density of filaments increases correspondingly and a qualitatively new feature in the pattern arises. Namely, filaments start to form linear objects (''chains''). Raising the voltage leads to generation of increasingly longer chains that finally extend across the complete active area [Figs. 3(b) and 3(c)]. In most cases, the long chains are ''connected'' to edges of the active area with both ends, while there can be also some short chains isolated from boundaries as well as single filaments. The chains touch boundaries at an angle of approximately 90°. This behavior is even more pronounced when the active area is not of a circular shape but is formed by straight boundaries. In Fig. 4 examples of a triangular and a rectangular active area are given. We note also that independent of the actual shape and size of the active area, the chains arrange in a way that they try to align parallel to neighboring chains. The distance between adjacent chains at the described experimental conditions is of the order of 5 mm and is virtually independent of control parameters.

Like single filaments, chains are not fixed to certain positions in the gas-discharge area and they are not rigid objects. In the course of time (i.e., on the scale of seconds), they can bend and twist. Also, they can break up at some point along

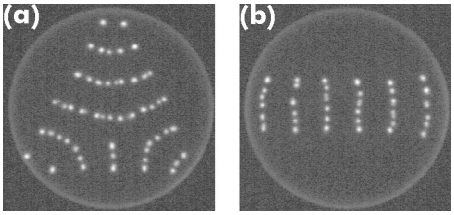

FIG. 4. Current density distributions on active areas of which the boundaries consist of straight lines: triangular (a) and a rectangular (b) geometry. The geometry has been defined by a mask prepared for the incident radiation falling on the semiconductor electrode. The circular area has a diameter of 30 mm. In both cases the parameters are $U_0=833$ V, $\varphi=0.03$ $[\sigma_{\mathrm{GaAs}}=0.50\times10^{-7}\ (\Omega\ \mathrm{cm})^{-1}]$, and $p=40$ hPa.

a chain and be split into several parts. But at the same time, new chains are formed that have the same characteristic features as their predecessors. A further increase in the supply voltage accompanied by an increase of the density of filaments leads to a situation where filaments no longer organize themselves in ''parallel'' chains [Fig. 3(d)]. Now chains do not maintain a fixed distance to each other any longer and they may even be connected, thus generating a kind of net structure. Finally chains disappear completely and filaments are scattered across the active area in an arbitrary manner [Figs. 3(e) and 3(f)]. These stages are comparable to those observed at lower voltages before the formation of chains [cf. Fig. 3(a)]. Now, however, we have a much larger density of filaments. Raising the voltage even more results in the formation of a state, where the complete active area is covered with filaments in an almost uniform manner [Figs. 3(g) and 3(h)]. When the system is filled up with filaments, a further increase in the supply voltage does not enlarge their number. Instead, this increase is accompanied by the increase of the filaments' speed. At this stage, images of the discharge glow taken with $t_{exp}=40$ ms show a smeared discharge radiation density distribution [Fig. 3(i)]. As a consequence the dynamics of filaments cannot be followed any more by means of a conventional video technique.

To analyze the spatial order in filamentary patterns, the spatial correlation of filaments has been evaluated. For this, the pair correlation function has been calculated from the discharge radiation density distribution. At first the positions of filaments were determined. In the algorithm, objects in an image of the discharge glow are identified as filaments when their brightness exceeds a certain threshold. For a given filament the number n_r of filaments between distances r and $r+\Delta r$ from the primary one is counted, where $\Delta r=0.09$ mm is determined by the resolution of the camera that has been used. For the calculation, only filaments inside a reduced area around the center of the active area are taken into account. The diameter of this reduced area is 12.5 mm, which is half of the total diameter of the active area that in this case is $D=25$ mm. The maximum distance r_{max} of analyzed pairs is set at $D/4=6.25$ mm to ensure that the vicinity of each filament considered lies completely in the active area of the system. Now n_r is determined for each filament on the reduced area. This procedure was repeated for a sequence of 250 pictures and finally averaged. This gives n_r

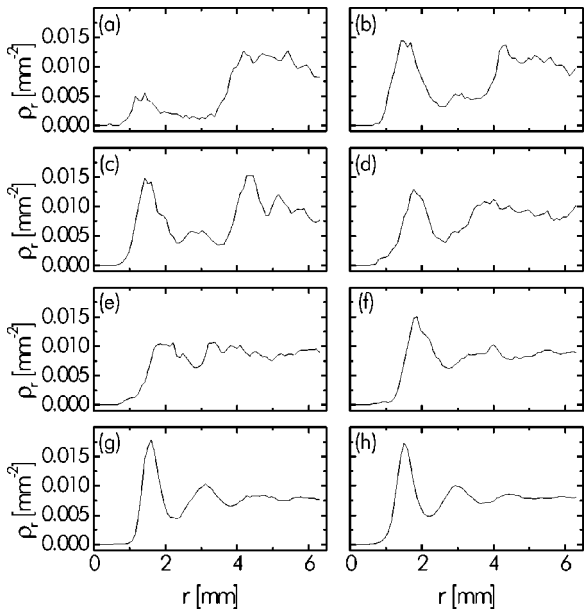

FIG. 5. Pair correlation functions ρ_r for filamentary states shown in Figs. 3(a)–3(h). The respective correlation functions are marked with the same letters as in Fig. 3.

$=p_r(2\pi r\Delta r)$ from which it is easy to calculate p_r. From p_r we obtain the normalized probability ρ_r by division with the average number of filaments within the reduced area. ρ_r is the probability density to find a filament at distance r from a given filament. We refer to ρ_r as the pair correlation function. The correlation functions for the filamentary states shown in Figs. 3(a)–3(h) are presented in Fig. 5 where they are denoted by respective letters. In Fig. 5(a), ρ_r has a small peak at $r\approx 1.5$ mm that indicates the tendency for formation of pairs of filaments (this can also be seen in the corresponding image). The formation of filamentary chains leads to the development of a second peak in the correlation function at $r\approx 4.3$ mm [Fig. 5(b)] that becomes even more expressed when the chains are fully developed [Fig. 5(c)]. This value is in good agreement with the distance between neighboring chains of filaments. The existence of the pronounced peak at small values of r indicates the presence of ordering of filaments along a chain. When chains are destroyed, the second peak disappears while the first one diminishes [Fig. 5(d)] until it also vanishes [Fig. 5(e)]. In this case, ρ_r has an almost constant value at distances that are larger than the minimum distance that is $r\approx 1.7$ mm. When the density of filaments grows even further, a new regularity develops. The filaments tend to maintain a fixed minimum distance, see Fig. 5(f), where a new peak at $r\approx 1.8$ mm has emerged. While raising the voltage further, this peak becomes higher and narrower while it is shifted to smaller values of r, which is approximately 1.5 mm in Fig. 5(h). When the active area of the gas-discharge domain is densely covered with filaments, the respective correlation functions ρ_r [Figs. 5(g) and 5(h)] have a characteristic shape. Besides the highest peak at small r that evidences the strong correlation between spatial positions of adjacent filaments, there is also a well-pronounced peak at twice this distance.

The sequence of filamentary states shown in Fig. 3 reveals

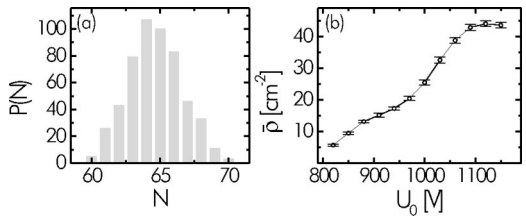

FIG. 6. (a) Typical shape of the frequency distribution $P(N)$ of number of filaments N that can be registered in the gas discharge area at fixed values of control parameters. The presented data are obtained as a result of the processing of 500 subsequent half-pictures of the discharge glow taken with $f_{rep}=50$ Hz and $t_{exp}=20$ ms. (b) Dependence of the average density of filaments $\bar{\rho}$ on the feeding voltage U_0. The error bars indicate the standard deviation in filament density due to fluctuations of their number. The parameters are $\varphi=0.05$ [$\sigma_{\mathrm{GaAs}}=0.65\times 10^{-7}$ $(\Omega\ \mathrm{cm})^{-1}$], $D=25$ mm, and $p=42$ hPa. The representative distribution shown in (a) has been measured at a voltage of $U_0=880$ V.

that while raising the voltage U_0 the number N of filaments grows. To count the number of filaments at a given set of parameters and evaluate the corresponding fluctuation, the same algorithm as for the determination of positions of filaments has been used. It turns out that the number of filaments undergoes temporal fluctuations at fixed parameters. To describe these fluctuations, a sequence of 250 pictures taken during the period of time of 10 s has been evaluated for each set of parameters. In a first step, the video pictures have been divided into their two half-frames (each with $t_{exp}=20$ ms), so that the number of evaluated half-frames is actually $B=500$. Finally, the number of images $P(N)$ containing N filaments is determined. For the state that is represented by the snapshot in Fig. 3(c), the distribution $P(N)$ is shown in Fig. 6(a) as a representative result. In all the other states illustrated in Fig. 3, the distributions have a similar shape, meaning that they have a distinct maximum and a certain breadth. From these distributions the average number of filaments $\bar{N}=\Sigma_{N=0}^{\infty}NP(N)/B$ has been determined while the fluctuations are characterized by the standard deviation $\sigma=[\Sigma_{N=0}^{\infty}(N-\bar{N})^2P(N)/B]^{1/2}$. To be more general, the result in Fig. 6 is given by using the average density of filaments $\bar{\rho}=\bar{N}/(\pi D^2/4)$. The error bars indicate the corresponding fluctuation in the density. The minimum density of filaments calculated from Fig. 6(b) is about 5 cm^{-2} and it grows monotonously with the voltage until it reaches saturation at about 43 cm^{-2}. This level indicates the state where the active area is covered with filaments to the maximum extent. As it has been pointed out above and as it is demonstrated in Fig. 3(i), a further rise in voltage does not lead to an increase in number of filaments but to an increase in their velocity.

The number of filaments fluctuates in time due to their generation and disappearance processes. In all experimental runs, only one type of generation process has been observed. This is illustrated by the sequence of pictures in Fig. 7, where the region of interest is marked by a white circle. A new filament is created by the splitting of an existing one. In Fig. 7(a), this process has just begun. The primary filament

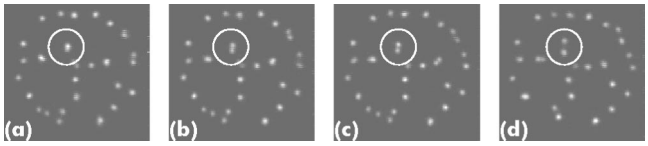

FIG. 7. Generation of a second filament due to splitting of a primary one. The distance in time between pictures (a) and (b) and between pictures (c) and (d) is 40 ms, the distance between pictures (c) and (d) is 160 ms. The parameters are $U_0=935$ V, $\varphi=0.043$ [$\sigma_{\mathrm{GaAs}}=0.60\times10^{-7}$ $(\Omega\ \mathrm{cm})^{-1}$], $p=60$ hPa, and $t_{exp}=40$ ms. The active area has a diameter of $D=13$ mm.

has altered its circular shape to an elliptical shape. In the next step (40 ms later), the ellipsis became stretched [Fig. 7(b)] and another 40 ms later, the deformed filament has split up and two filaments are distinguishable [Fig. 7(c)]. As time goes on, the distance between these two filaments becomes larger as can be seen in Fig. 7(d). This snapshot has been taken 160 ms after the previous one. The splitting process is the reason for the existence of pairs of filaments that can be observed, e.g., in Fig. 3(a). These pairs are not created through combination of two single filaments but exist as a transient state after a splitting event has occurred.

The collapse of filaments also proceeds through a single process. This scenario is documented by the sequence of pictures in Fig. 8 where the region of interest is again marked by a white circle. The experimental conditions are the same as those corresponding to the data of Fig. 7. The brightness of the marked filament decreases in states represented by the sequence of snapshots Figs. 8(a)–8(c), until finally the filament has disappeared [Fig. 8(d)]. The annihilation of a filament seems not to be triggered by any interaction with other filaments. It happens in an unpredictable manner: A filament can disappear just after it has been generated by the splitting process described above, but it can also exist for several seconds. Both cases can be observed experimentally.

Investigating the total current I through the gas-discharge device, we find a significant time dependence. An example of a typical time series is presented in Fig. 9. It belongs to a situation with developed chains of filaments similar to that illustrated by Fig. 3(c). The recorded global current I exhibits a nonperiodic succession of narrow peaks, each peak has a width of about 300 ns. Most of the peaks have approximately the same height (in the given example about 1 mA). The time series of the other states represented by the sequence of pictures in Fig. 3 resemble that of Fig. 9 but, depending on the parameter set, the succession of peaks on the time axis

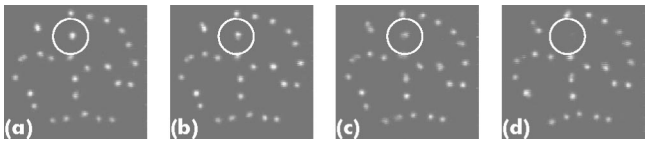

FIG. 8. Annihilation of a filament. The experimental conditions are the same as in Fig. 7. The repetition rate of the frames is $f_{rep}=25$ Hz. The further parameters are $U_0=935$ V, $\varphi=0.043$ [$\sigma_{\mathrm{GaAs}}=0.60\times10^{-7}$ $(\Omega\ \mathrm{cm})^{-1}$], $p=60$ hPa, and $t_{exp}=40$ ms. The active area has a diameter of $D=13$ mm.

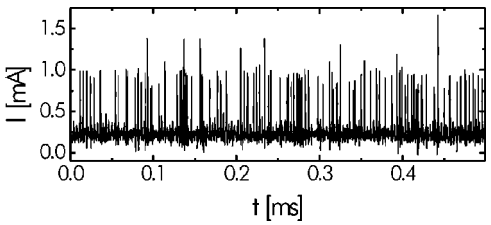

FIG. 9. An example of a typical time series of the global current for a filamentary state characterized by long chains of filaments like that shown in Fig. 3(c). The average discharge current is 0.25 mA. The parameters are $U_0=846$ V, $\varphi=0.09$ [$\sigma_{\mathrm{GaAs}}=0.95\times10^{-7}$ $(\Omega\ \mathrm{cm})^{-1}$], $D=25$ mm, and $p=60$ hPa.

varies. The frequency of peaks is larger the higher the average number of filaments in the discharge, while the amplitude of peaks is virtually equal in all states. The appearance of such dynamics of the global current suggests that each discharge current peak is related to the ignition of a filament, which then exists only for a very short period of time. The fact that filaments can be seen on a video camera picture, which is actually the result of the integration of the discharge glow over several breakthroughs, leads to the conclusion that a subsequent breakthrough is supported in regions where a filament did exist before. To verify the above conclusions directly, one has to investigate the temporal behavior of a single filament. This can be done by restricting the active area in a way that only one filament can exist. Practically, this is accomplished by irradiating only a small region of the semiconductor. This region can still be chosen larger than one filament—which has typically a diameter of the order of 0.6 mm—thereby ensuring that the filament is still not essentially influenced by the boundaries of the system. An example of the time series for such a situation is shown in Fig. 10(a). This result illustrates that the dynamics of a single filament actually consists of a sequence of breakthroughs that are relatively short in time as compared to the characteristic time interval between them. It is also revealed that the breakthroughs do not occur periodically, although Δt lies in the limited range of 0.02–0.033 ms [cf. Fig. 10(b)].

By using a fast light-intensifying camera, it is possible to record pictures of the gas-discharge domain in the studied system on the time scale of the repetition rate of filaments.

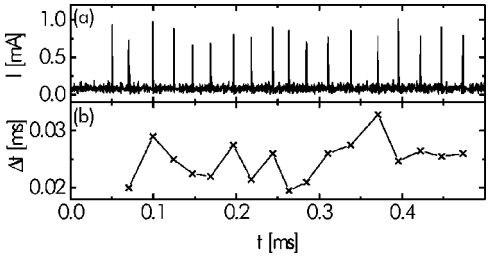

FIG. 10. An example of the time series of the discharge current (a) and the time Δt between successive current spikes (b) for the situation of a restricted active area with appearance of only one filament. The average discharge current is 0.09 mA. The parameters are $U_0=854$ V, $\varphi=0.12$ [$\sigma_{\mathrm{GaAs}}=1.18\times10^{-7}$ $(\Omega\ \mathrm{cm})^{-1}$], $D=3$ mm, and $p=60$ hPa.

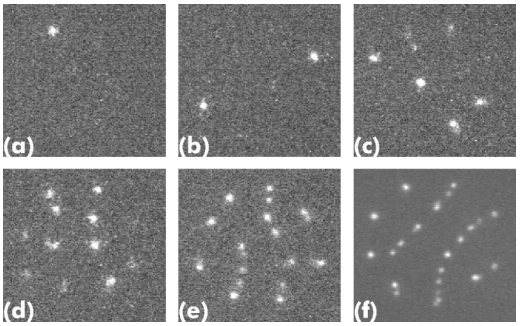

FIG. 11. Records of the light density distribution of the gas-discharge with short exposure times: (a),(b) $t_{exp}=3\ \mu$s, (c) $t_{exp}=10\ \mu$s, (d) $t_{exp}=30\ \mu$s, and (e) $t_{exp}=300\ \mu$s. For comparison, a video camera picture taken under the same experimental conditions is presented (f). The parameters are $U_0=908$ V, $\varphi=0.04$ [$\sigma_{\mathrm{GaAs}}=0.58\times10^{-7}\ (\Omega\ \mathrm{cm})^{-1}$], and $p=60$ hPa, the active area has a diameter of $D=15$ mm.

Such pictures with short exposure times t_{exp} are shown in Fig. 11, where the active area is smaller than that corresponding to Fig. 3. Due to the short exposure time, a high amplification of the discharge glow is necessary and, therefore, the presented snapshots are more noisy. For comparison, a video camera picture with $t_{exp}=40$ ms is also included [Fig. 11(f)]. In the case of $t_{exp}=3\ \mu$s, there are either one or two filaments visible [Figs. 11(a) and 11(b)]; at the same time, for a given exposure time, it is possible to get pictures with no filaments at all. In contrast to a video camera picture, in these cases of short exposure time, only one breakthrough per filament is registered. When t_{exp} is made longer, more and more breakthroughs that occur at different positions of the active area can be recorded [Figs. 11(c) and 11(d)]. Until now we have found no temporal correlation between spatially correlated filaments, e.g., the pictures reveal that two adjacent filaments (for example, two filaments in a chain) are not correlated in time. At $t_{exp}=300\ \mu$s, the picture of the discharge virtually shows no difference to a corresponding video camera picture.

III. SUMMARY AND DISCUSSION

In the present work, electrical transport processes in a planar dc-driven gas-discharge system with a high resistance semiconductor electrode are studied. The discharge in nitrogen at moderate pressures is applied. The main pattern-formation phenomenon observed is the formation of a multifilamentary current state. It has been shown that filamentary patterns are essentially nonstationary; individual current filaments are formed by repetitive electrical breakdown of the gas layer. The experimental data suggest that filamentary patterns arise as a result of losing the stability of the spatially homogeneous stationary discharge. The instability appears at the increase of current density in the device above some threshold value. Such current control in the considered case is mainly provided by the variation of the feeding voltage. In the course of the transition from the stationary homogeneous state to a filamentary pattern, some intermediate stage in pattern formation process is observed. At this stage, local filamentarylike breakdown arising on the low-current stationary-homogeneous background generates waves that propagate across the active area of the system. The waves exist in a rather narrow range of control parameters. A further increase in current, as compared to the critical value for the instability, gives rise to a pattern composed of filaments. Filaments can exhibit a pronounced cooperative behavior resulting in formation of spatially extended structures (''chains'') with two characteristic spatial scales. To be more explicit, the distance between neighboring filaments in a chain is essentially smaller as compared with the distance between adjacent chains in a pattern. As a result, an anisotropic pattern is organized in the two-dimensional system.

The formation of chain patterns and their intrinsic anisotropy have been demonstrated to be quite a robust property of the system. More explicitly, a change in the geometry of the active areas of the device is accompanied by a spatial reconstruction of the chain pattern, while its internal symmetry is retained. By varying the control parameters, an increasing number of filaments can be generated in the system. With U_0 being further increased, chains are destroyed and the resulting pattern reminds us of the liquid state.

In relation to these findings we notice that the formation of filamentary patterns in dc-driven ''semiconductor-discharge gap'' systems have been earlier studied in, e.g., [16,19]. In this work nitrogen has also been applied. The essential difference between the present and previous experimental conditions is, however, that the discharge system in [16,19] was kept cooled down to about 90 K. There, filamentary patterns were composed of stationary filaments. Formation of these structures could be satisfactorily described in terms of the Turing instability of the homogeneous discharge state.

In the present work, a qualitatively different filamentation process takes place where individual filaments oscillate in time. The recent investigation of the present system at slightly different parameters [22] has revealed the existence of a Hopf bifurcation from a stable stationary homogeneous discharge to an oscillatory mode, the oscillations being in phase all over the total active area of the system. These two phenomena (the oscillatory mode of the spatial homogeneous discharge and the existence of patterns composed of oscillating filaments) seem to be closely related. It is tentative to suggest that the appearance of patterns composed of oscillatory filaments is due to the fact that the system becomes unstable to both Hopf and Turing modes [26].

The most intriguing phenomenon that is observed is the formation of anisotropic chain patterns that are characterized by two spatial scales. At the moment, the peculiarities in the filaments' interaction that are responsible for the formation of chain structures are not clear. An understanding of this phenomenon requires, first of all, a description of the spatiotemporal dynamics of a solitary filament. We believe, however, that the main driving force for the formation of oscillating filamentary patterns is the Hopf bifurcation in the system [22].

We would like to add also that filamentary patterns of various types have been studied in planar dielectric barrier

gas-discharges [15,27–29]. These discharges can be driven only by an ac voltage. Filaments in these systems oscillate in a coherent way with the period of the driving force. As far as we know, ac-driven dielectric barrier discharges do not demonstrate filamentary chain patterns that would be similar to those that are quite robust in our case.

ACKNOWLEDGMENTS

We would like to thank S. Flothkötter for programming the filament-counting algorithm. The support of the present work by the Deutsche Forschungsgemeinschaft (DFG) is gratefully acknowledged.

[1] H. Haken, *Synergetics—An Introduction* (Springer, Berlin, 1978).
[2] M.C. Cross and P.C. Hohenberg, Rev. Mod. Phys. **65**, 851 (1995).
[3] F.H. Busse and S.C. Müller, *Evolution of Spontaneous Structures in Dissipative Continuous Systems* (Springer, New York, 1998).
[4] *Chemical Waves and Patterns*, edited by R. Kapral and K. Showalter (Kluwer, Dordrecht, 1995).
[5] R. Imbihl and G. Ertl, Chem. Rev. **95**, 697 (1995).
[6] V.S. Zykov and S.C. Müller, Physica D **97**, 322 (1996).
[7] H. Meinhardt, *Models of Biological Pattern Formation* (Academic Press, London, 1982).
[8] J.D. Murray, *Mathematical Biology* (Springer, Berlin, 1989).
[9] H.-G. Purwins, Yu.A. Astrov, and I. Brauer (unpublished).
[10] G. Ahlers, Physica D **51**, 421 (1991).
[11] B.S. Kerner and V.V. Osipov, *Autosolitons: A New Approach to Problems of Self-Organization and Turbulence* (Kluwer, Dordrecht, 1994).
[12] M. Bode and H.-G. Purwins, Physica D **86**, 53 (1995).
[13] C. Radehaus, R. Dohmen, H. Willebrand, and F.-J. Niedernostheide, Phys. Rev. A **42**, 7426 (1990).
[14] H. Willebrand, T. Hünteler, F.-J. Niedernostheide, R. Dohmen, and H.-G. Purwins, Phys. Rev. A **45**, 8766 (1992).
[15] E. Ammelt, D. Schweng, and H.-G. Purwins, Phys. Lett. A **179**, 348 (1993).
[16] Yu.A. Astrov, E. Ammelt, S. Teperick, and H.-G. Purwins, Phys. Lett. A **211**, 184 (1996).
[17] E. Ammelt, Yu.A. Astrov, and H.-G. Purwins, Phys. Rev. E **55**, 6731 (1997).
[18] Yu.A. Astrov and Yu.A. Logvin, Phys. Rev. Lett. **79**, 2983 (1997).
[19] E. Ammelt, Yu.A. Astrov, and H.-G. Purwins, Phys. Rev. E **58**, 7109 (1998).
[20] Yu.A. Astrov, I. Müller, E. Ammelt, and H.-G. Purwins, Phys. Rev. Lett. **80**, 5341 (1998).
[21] H.-G. Purwins, C. Radehaus, T. Dirksmeyer, R. Dohmen, R. Schmeling, and H. Willebrand, Phys. Lett. A **136**, 480 (1989).
[22] C. Strümpel, Yu.A. Astrov, and H.-G. Purwins, Phys. Rev. E **62**, 4889 (2000).
[23] Material supplied by the Freiberger Compound Materials GmbH (Germany) has been used.
[24] Yu.P. Raizer, *Gas Discharge Physics* (Springer, Berlin, 1991).
[25] Movies illustrating the dynamics of some spatial inhomogeneous states can be found at http://www.uni-muenster.de/Physik/AP/Purwins/gas.
[26] M. Meixner, A. De Witt, S. Bose, and E. Schöll, Phys. Rev. E **55**, 6690 (1997).
[27] D.G. Boyer and W.A. Tiller, Appl. Phys. Lett. **41**, 28 (1982).
[28] W. Breazeal, K.M. Flynn, and E.G. Gwinn, Phys. Rev. E **52**, 1503 (1995).
[29] I. Brauer, M. Bode, E. Ammelt, and H.-G. Purwins, Phys. Rev. Lett. **84**, 4104 (2000).